Anisotropic magnetoresistance in manganites: experiment and theory

Anisotropic magnetoresistance in manganites: experiment and theory

J D Fuhr, M Granada, L B Steren and B Alascio

Centro Atómico Bariloche, CNEA, CONICET, Bustillo 9500, (8400) San Carlos de Bariloche, Argentina

Abstract
We present measurements of the anisotropic magnetoresistance (AMR) of $La_{0.75}Sr_{0.25}MnO_3$ films deposited on (001) $SrTiO_3$ substrates, and a model that describes the experimental results. The model, based on the electronic structure of manganites plus the spin–orbit coupling, correctly accounts for the dependence of the AMR on the direction of the current to the crystalline axes. We measure an AMR of the order of 10^{-3} for the current I parallel to the [100] axis of the crystal and vanishing AMR for $I \parallel [110]$, in agreement with the model predictions. Further, we calculate the planar Hall effect and show its connection to AMR.

(Some figures in this article are in colour only in the electronic version)

1. Introduction

Since the discovery of colossal magnetoresistance (CMR) in doped manganites, they have been investigated thoroughly [1–5], including the anisotropic magnetoresistance (AMR) that may lead to application of these materials in electronics [6–11]. While AMR has been observed in both conventional metallic systems and CMR materials, their sign and temperature dependences are quite different. For polycrystalline ferromagnetic metals and alloys in the magnetically ordered state it has been found that the resistivity depends only on the angle θ between the magnetization M and the electric current I. This dependence has the form [12]

$$\rho(\theta) = \rho_\perp + (\rho_\parallel - \rho_\perp)\cos^2\theta \qquad (1)$$

$\rho_\parallel$ and $\rho_\perp$ being the resistivity measured with current flowing parallel or perpendicular to the magnetization, respectively. In most conventional metals the AMR, defined as

$$\rho_{AMR} = \frac{(\rho_\parallel - \rho_\perp)}{(\frac{1}{3}\rho_\parallel + \frac{2}{3}\rho_\perp)}$$

is positive [13] and decreases with decreasing magnetization or increasing temperature. On the other hand, in manganites it is an order of magnitude lower, of opposite sign, and its temperature dependence is non-monotonic [6–11]. These differences point to the fact that different mechanisms must be in action in the different materials. The model proposed by Campbell *et al* [13] based on the scattering of s waves on the d sites of the material has been successful in the understanding of AMR in metallic alloys, describing properly the effects of impurity concentration and temperature dependence. This s–d model has also been mentioned in reference to AMR measurements in manganites, in spite of the fact it is not appropriate to describe these materials where the carriers, electrons or polarons, move by hopping between the d states of the transition metal. Therefore, it is necessary to develop an appropriate theory to describe AMR in manganites.

Here, we present measurements on manganite films and a model based on the effects of spin–orbit (SO) coupling on the electronic structure of manganites. To calculate the transport properties, we resort to the usual transport formula for Fermi quasi-particles. Our model succeeds in describing the experimental results, including the dependence of the AMR on the direction of the current to the crystalline axes.

2. Experiment

The ferromagnetic manganite $La_{0.75}Sr_{0.25}MnO_3$ (LSMO) presents a nearly cubic perovskite structure [14] that makes this system ideal for comparison with our calculations, which are developed for a cubic lattice of Mn ions. The samples were deposited on (001) $SrTiO_3$ (STO) substrates by dc sputtering. The films grow textured along the (001) direction, as confirmed by x-ray diffraction experiments [15]. The STO substrate, having a lattice constant similar to that of LSMO, induces little distortion on the film compared to the bulk manganite.

The $La_{0.75}Sr_{0.25}MnO_3$ films are metallic (figure 1(a)) and ferromagnetic below room temperature. The low temperature
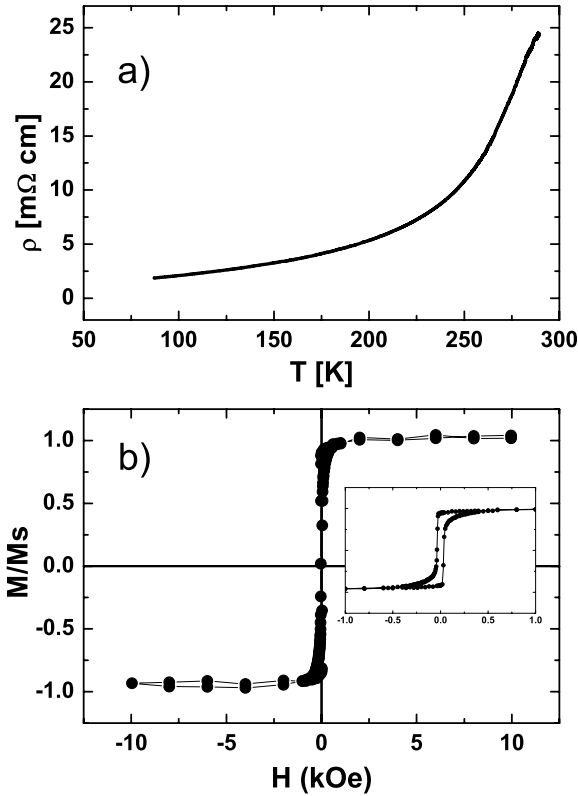
Figure 1. Characteristics of an 80 nm LSMO film. (a) Resistivity versus temperature. (b) Magnetization loop measured at 85 K with the magnetic field applied in the plane of the sample.
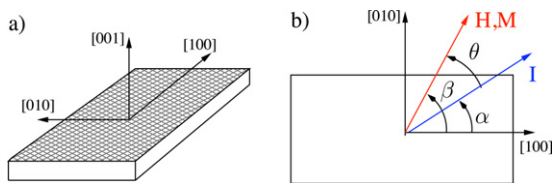

Figure 2. (a) Scheme of the sample indicating the direction of the crystalline cubic axis. (b) Top view with the definition of the angles for the current I and the magnetic field H (magnetization M).

Figure 3. Normalized resistivity measured at $T = 88$ K with the current I applied parallel to the crystalline direction [100] for films of three different thicknesses (20, 30 and 60 nm). Hollow circles represent the resistivity measurements with $I \parallel$ [110] for the 20 nm sample. θ is the angle measured between the direction of the electrical contacts and the applied magnetic field ($H = 10$ kOe). A fit with expression (1) is also shown (lines).

resistivity is typical of metallic manganites, ensuring a good quality film. Magnetization loops, measured at 85 K in a vibrating sample magnetometer (VSM), show that the films are fully saturated for magnetic fields larger than 1 kOe applied in the plane of the films (figure 1(b)). The magnetism of the films has been studied by ferromagnetic resonance experiments, and typical anisotropy fields of the order of 0.5 kOe have been estimated from the measurements performed at 80 K [16].

We present electrical transport measurements performed on 2.5×5.0 mm^2 films of different thicknesses, using the longitudinal four-lead configuration with the gold sputtered contacts on the plane of the films. The diameter of the sputtered gold contacts is 0.5 mm and the internal distance between the contacts for voltage measurements is 0.34 mm. As we focus on the AMR, all the measurements were carried out with a magnetic field of $H = 10$ kOe applied parallel to the film surfaces, which is sufficient to saturate the sample
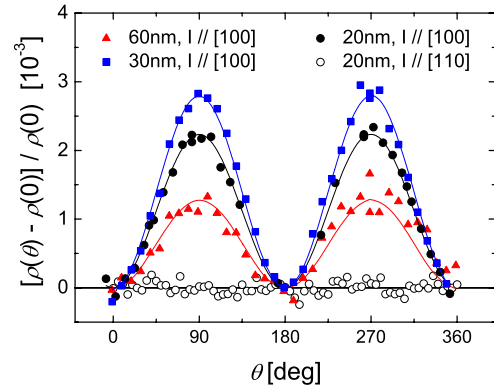
magnetization. Therefore, the angle θ between the electrical current I and the magnetic field is the same as the angle between I and the magnetization M (figure 2). The current I was aligned either parallel to the [100] or the [110] LSMO crystallographic axis.

Figure 3 shows the normalized resistivity $[\rho(\theta) - \rho(0)]/\rho(0)$ measured at $T = 88$ K with the current applied parallel to the crystalline direction [100] showing agreement with (1) and previous AMR measurements [9, 10]. We have measured the angular dependence of the AMR for films of different thickness and we have not found any monotonic dependence of the AMR on this parameter. Prompted by the prediction of vanishing AMR (see below), we also performed measurements with the current parallel to the [110] direction. The resulting AMR is displayed in figure 3 by empty circles, where we see negligible dependence of the resistivity on the magnetic field direction.

3. The model

In La$_{1-x}$Sr$_x$MnO$_3$, the Mn$^{3+/4+}$ ions form a nearly simple cubic lattice, with oxygen ions located between each pair of Mn neighbors and La/Sr ions at the body center of the cube. The octahedral symmetry around each Mn splits the 3d levels into a lower energy t$_{2g}$ triplet and a higher energy e$_g$ doublet. Due to Hund's rule, the three t$_{2g}$ orbitals are all singly occupied with their spins coupled to form the total spin $S = 3/2$ of ionic cores. The additional electrons on the Mn^{3+} sites occupy the e$_g$ orbitals and are itinerant due to the double exchange that transfers them from site to site. Due to the strength of the exchange term ($J \vec{S}_i \cdot \vec{\sigma}_i$), we consider each itinerant electron to align its spin parallel to the t$_{2g}$ electrons. As we are considering a fully saturated system, the localized spins of the t$_{2g}$ electrons, as well as the itinerant electrons, are all aligned with the external magnetic field. We then model the itinerant
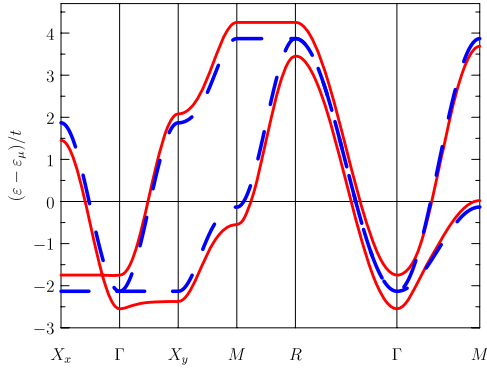
Figure 4. Band dispersion $\varepsilon_n(\vec{k})$ with spin–orbit (SO) coupling ($g/t = 0.2$, continuous line) and without SO coupling (dashed line). Two of the special points are labeled X_x ($\vec{k} = (\pi, 0, 0)$) and X_y ($\vec{k} = (0, \pi, 0)$) to emphasize that they become nonequivalent when SO coupling is included.

e_g electrons by a spinless Hamiltonian on a cubic lattice:

$$H = \sum_{\langle ij \rangle \alpha \beta} t_{ij}^{\alpha\beta} c_{i\alpha}^\dagger c_{j\beta} \qquad (2)$$

with $t_{ij}^{\alpha\beta}$ the hopping integrals that depend both on the type of orbital α, β and on the direction between neighboring sites i, j [17].

To account for the AMR, we include an in-site SO coupling. The degeneracy of the e_g orbitals ($|z\rangle = |3z^2 - r^2\rangle$, $|x\rangle = |x^2 - y^2\rangle$) is lifted. We start by discussing the effect of the SO coupling on the site energies. By symmetry, there is no coupling between $e_g\uparrow$ and $e_g\downarrow$ orbitals. Moreover, we take into account only the coupling between the $e_g\uparrow$ and $t_{2g}\uparrow$ orbitals (separated by a crystal field of $\sim$1.5 eV), and neglect the coupling with the $t_{2g}\downarrow$ orbitals (separated by $\sim$6 eV [18]). The character of the two, now not degenerate, orbitals ($|1\rangle$, $|2\rangle$) depends on the direction of the magnetic field. From second order perturbation theory, we obtain the shift and coupling of the two original e_g orbitals for the magnetization in a given direction (θ_B, ϕ_B), in spherical coordinates referred to axes parallel to the crystalline axes, as

$$H_{SO} = g \begin{pmatrix} 3\sin^2(\theta_B) & \sqrt{3}\sin^2(\theta_B)\cos(2\phi_B) \\ \sqrt{3}\sin^2(\theta_B)\cos(2\phi_B) & \sin^2(\theta_B) + 4\cos^2(\theta_B) \end{pmatrix} \qquad (3)$$

where $g = \lambda^2/\Delta_{CF}$, λ being the SO coupling constant and Δ_{CF} the crystal field splitting between t_{2g} and e_g orbitals. From this SO coupling, we can obtain the new energy levels ($\varepsilon_{1,2} = g(2 \mp \Delta)$) and the corresponding eigenvectors in each site

$$|1\rangle, |2\rangle = \frac{(a \mp \Delta)}{r_{1,2}}|z\rangle + \frac{b}{r_{1,2}}|x\rangle \qquad (4)$$

where $a = \sin^2(\theta_B) - 2\cos^2(\theta_B)$, $b = \sqrt{3}\sin^2(\theta_B)\cos(2\phi_B)$, $\Delta = \sqrt{a^2 + b^2}$ and $r_{1,2} = \sqrt{(a \mp \Delta)^2 + b^2}$. Therefore, the SO splitting is $\delta\varepsilon_{SO} = 2g\Delta$ and is determined by the magnetization direction (θ_B, ϕ_B).

The band dispersion $\varepsilon_n(\vec{k})$ is obtained by diagonalizing the total Hamiltonian $H(\vec{k}) + H_{SO}$, where $H(\vec{k})$ is the Fourier transform of equation (2):

$$H(\vec{k}) = t \begin{pmatrix} -\frac{1}{2}(\cos k_x + \cos k_y) - 2\cos k_z & \frac{\sqrt{3}}{2}(\cos k_x - \cos k_y) \\ \frac{\sqrt{3}}{2}(\cos k_x - \cos k_y) & -\frac{3}{2}(\cos k_x + \cos k_y) \end{pmatrix}. \qquad (5)$$

In figure 4 we show this band dispersion with SO coupling (continuous line) and without SO coupling (dashed line). In order to show the effect of the SO coupling, we used for this figure a value of $g/t = 0.2$, which is two orders of magnitude higher than the value used later in the AMR calculations to adjust to the experiments. We labeled two of the special points by X_x ($\vec{k} = (\pi, 0, 0)$) and X_y ($\vec{k} = (0, \pi, 0)$) to emphasize that they become nonequivalent when SO coupling is included.

Assuming now an isotropic relaxation time τ, the current density $\vec{j}$ for an applied electric field $\vec{E}$ is given by [19]

$$\vec{j} = e^2\tau \sum_n \int d^3k \, \frac{\partial f}{\partial \varepsilon_n(\vec{k})}[\vec{E} \cdot \vec{\nabla}\varepsilon_n(\vec{k})]\vec{\nabla}\varepsilon_n(\vec{k}), \qquad (6)$$

with $f(\varepsilon)$ the Fermi function. In terms of the conductivity tensor $\bar{\bar{\sigma}}$ with components

$$\sigma_{ij} = e^2\tau \sum_n \int d^3k \, \frac{\partial f}{\partial \varepsilon_n(\vec{k})} \frac{\partial \varepsilon_n(\vec{k})}{\partial k_i} \frac{\partial \varepsilon_n(\vec{k})}{\partial k_j}, \qquad (7)$$

the current density can then be written as

$$\vec{j} = \bar{\bar{\sigma}} \cdot \vec{E}. \qquad (8)$$

Due to the cubic symmetry of the system, all non-diagonal components of the conductivity tensor are equal to zero. The argument of the integral in equation (7) for σ_{xx} and σ_{yy} is shown in figure 5 as a density plot, in the (k_x, k_y) plane, for the magnetization in the $\hat{x}$ direction and $k_z = \pi/2$. For this figure, we again used large values for the SO coupling ($g/t = 0.2$) and the electronic temperature ($k_B T_e/t = 0.05$) to better visualize the effect. It shows that the integrand to obtain σ_{xx} (parallel to H) is larger than the corresponding value for σ_{yy}, leading to a lower resistivity.

In the experimental setup for a given applied current direction, two voltages can be measured. The voltage parallel to the current which is the usual one for studying the AMR, and the perpendicular one used for studying the planar Hall effect (PHE). From them, one obtains the longitudinal resistivity ρ_{long} and the transverse resistivity ρ_{trans}, which from the model can be calculated as

$$\rho_{long} = \frac{E_\parallel}{J} = \frac{\vec{E} \cdot \hat{j}}{J} \qquad (9)$$

$$\rho_{trans} = \frac{E_\perp}{J} = \frac{\vec{E} \cdot (\hat{n} \times \hat{j})}{J} \qquad (10)$$

where $\hat{n}$ is the film normal, and the direction of $\vec{E}$ is chosen in order to obtain the imposed direction of $\vec{j}$, i.e. $\vec{E} = \bar{\bar{\sigma}}^{-1} \cdot \vec{j}$.
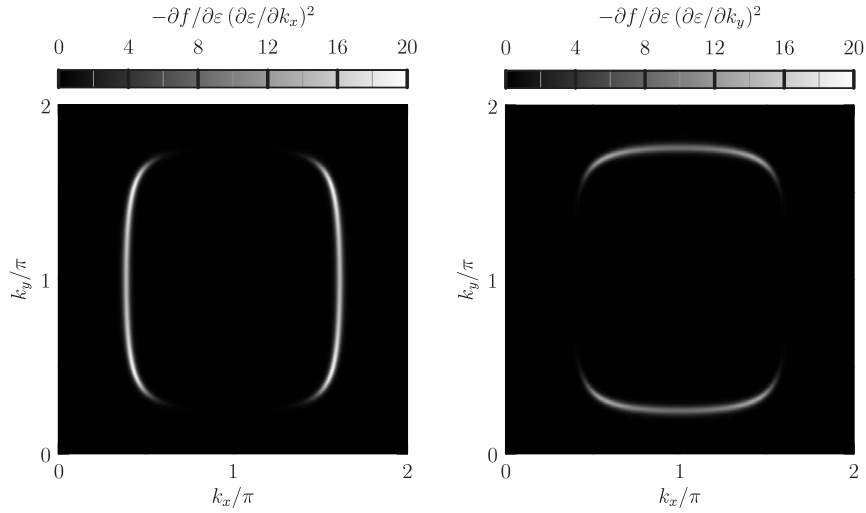
Figure 5. Density plot of the argument of the integral in (equation (7)) for H, M in the $\hat{x}$ direction, and $k_z = \pi/2$. It shows that the integrand to obtain σ_{xx} (parallel to H) is larger than the corresponding value for σ_{yy}, leading to a lower resistivity. We used large values for the spin–orbit coupling ($g/t = 0.2$) and the electronic temperature ($k_B T_e/t = 0.05$) to better visualize the effect.

4. Results

For the calculations, we took as the energy reference the hopping t between two $|z\rangle$ orbitals in the $\hat{z}$ direction. Therefore, the only free parameter is the constant $g/t = \lambda^2/(\Delta_{CF} t)$. We took $g/t = 0.001$ to approximately fit the experimental results. This value is perfectly consistent with the atomic value of the LS coupling ($\lambda = 0.04$ eV), the crystal field splitting ($\Delta_{CF} = 1.5$ eV) and a hopping of $t = 0.4$ eV [6].

We first considered the case with the magnetic field rotating in the $\hat{x}$–$\hat{y}$ plane ($\theta_B = \pi/2$, $\phi_B = \beta$), which corresponds to (001) textured films. In this case the relevant parameters are the conductivities σ_{xx} and σ_{yy} which are different only when SO coupling is taken into account. Therefore, we write these conductivities in terms of the mean value $\sigma_m = (\sigma_{xx} + \sigma_{yy})/2$ and the difference $\Delta\sigma = (\sigma_{xx} - \sigma_{yy})/2$. In order to show the dependence of the resistivities ρ_{long} and ρ_{trans} on the current and magnetization directions, we take the limit of (9) and (10) for $\Delta\sigma \ll \sigma_m$, obtaining

$$\rho_{long} = \frac{1}{\sigma_m}\left[1 - \cos(2\alpha)\frac{\Delta\sigma}{\sigma_m} + \mathcal{O}\left(\left(\frac{\Delta\sigma}{\sigma_m}\right)^2\right)\right] \quad (11)$$

$$\rho_{trans} = \frac{1}{\sigma_m}\left[\sin(2\alpha)\frac{\Delta\sigma}{\sigma_m} + \mathcal{O}\left(\left(\frac{\Delta\sigma}{\sigma_m}\right)^2\right)\right] \quad (12)$$

where α gives the current direction with respect to the [100] axis, and *a priori* both σ_m and $\Delta\sigma$ can depend on the magnetization direction as given by the angle β to the [100] axis (see figure 2). From the numerical calculations, we obtained a constant σ_m and a dependence $\Delta\sigma = \Delta\sigma_0 \cos(2\beta)$, as can be seen in figure 6. We finally obtain for the resistivities, within the first order in $\Delta\sigma/\sigma_m$:

$$\rho_{long} = \rho_m[1 - A\cos(2\alpha)\cos(2\beta)] \quad (13)$$

$$\rho_{trans} = \rho_m[A\sin(2\alpha)\cos(2\beta)] \quad (14)$$
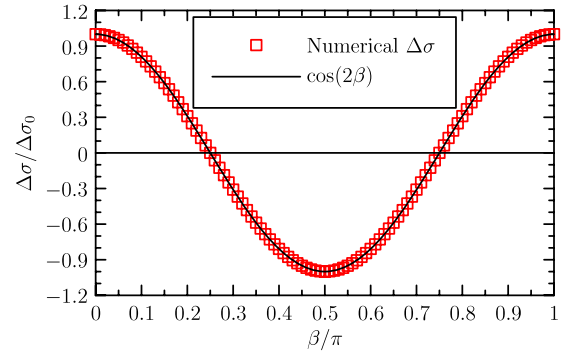

Figure 6. Numerical results for $\Delta\sigma$ as a function of magnetization direction β, compared with the simple form $\cos(2\beta)$.

with $\rho_m = 1/\sigma_m$ and $A = \Delta\sigma/\sigma_m$, which takes the value $A \simeq 0.001\,47$ for the parameters we used. The results obtained in (13) and (14) for ρ_{long} and ρ_{trans} can be directly compared with equations (5) and (6) of [11] (note the differences in notation: (α, β) here correspond to (θ, α) in [11]). In fact, the expressions are the same if in [11] the conditions $A = B$ and $C = 0$ are fulfilled, which approximately occurs for $T \simeq 125$ K.

In order to compare with the experimental results shown in figure 3, we calculated the normalized longitudinal resistivities $[\rho(\theta) - \rho(0)]/\rho(0)$ as a function of the magnetization direction θ from the corresponding current directions ([100] and [110]). We show the calculated AMR in figure 7(a). Although these calculations were carried out numerically, the result for $I \parallel [100]$ is indistinguishable from a $\cos^2\theta$ dependence like that of (1) and the limit obtained in (13). This is again in agreement with our experimental results and those of [9–11]. We can also see that the resistivity for $I \parallel [110]$ does not depend on the direction of the magnetization, also in agreement with the measurements shown in figure 3, and can be clearly seen in (13) which for $\alpha = \pi/4$ reduces to $\rho_{long} = \rho_m$. This
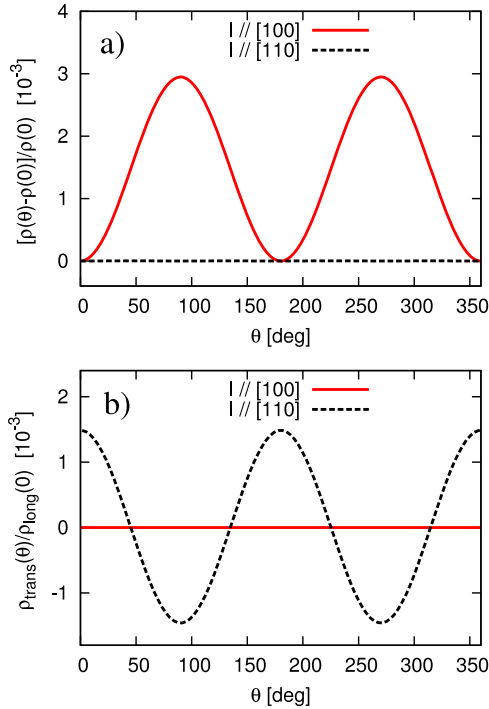
Figure 7. Calculated normalized longitudinal (a) and transverse (b) resistivities for (001) films and the current flowing in the [100] and the [110] directions, as a function of the magnetic field direction θ measured from the corresponding current direction. The magnetic field rotates in the $\hat{x}-\hat{y}$ plane.
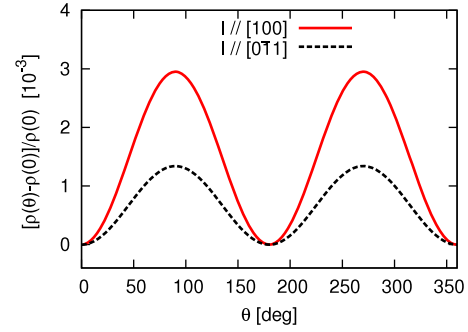

Figure 8. Calculated normalized longitudinal resistivity for (011) films and the current flowing in the [100] and the [0$\bar{1}$1] directions, as a function of the magnetic field direction θ measured from the corresponding current direction. The magnetic field rotates in the [100]–[0$\bar{1}$1] plane.

result can be understood from the $\cos^2(\beta)$ dependence of the resistivity, the cubic symmetry, and the dependence of resistivity with current direction given by equation (9). In fact, from the cubic symmetry we have that $\rho_{\rm long}^{[010]}(\beta) = \rho_{\rm long}^{[100]}(\beta - \pi/2)$, and from equation (9) we can obtain $\rho_{\rm long}^{[110]}(\beta) = (\rho_{\rm long}^{[100]}(\beta) + \rho_{\rm long}^{[010]}(\beta))/2$. Then, since $\rho_{\rm long}^{[100]}(\beta) = \rho_{\rm m} + \Delta\rho(\cos^2\beta - 1/2)$ with $\Delta\rho = -2\rho_{\rm m}A$, we finally obtain $\rho_{\rm long}^{[110]}(\beta) = \rho_{\rm m}$ which does not depend on the magnetization direction.

We also calculated the transverse resistivity $\rho_{\rm trans}$, as given by equation (10), which leads to the planar Hall effect. The results are shown in figure 7(b) for the current in the [100] and [110] directions. We see the opposite behavior to that for $\rho_{\rm long}$, the PHE is maximum for $I \parallel$ [110] and vanishes for $I \parallel$ [100]. This is in agreement with recent results of Bason *et al* [11].

Finally, we calculated the AMR for the case of (011) textured films. In this case, the magnetic field now rotates in the [100]–[0$\bar{1}$1] plane and we calculate the conductivity in the two nonequivalent directions [100] and [0$\bar{1}$1]. We show the calculated AMR in figure 8, where as before the angle θ of the magnetic field is measured from the current direction. It is difficult to compare this prediction with previous experimental results [8, 9], since the behavior of the AMR strongly depends on the samples.

5. Conclusions

We have measured the low temperature AMR of (001) La$_{0.75}$Sr$_{0.25}$MnO$_3$ films. We have also formulated a model to calculate AMR in manganites, which explains satisfactorily the sign, magnitude and angular dependence for the current along the [100] axis. It also led us to predict and measure a vanishing AMR when the current flows in the [110] direction. From the calculation of the conductivity tensor, we have also obtained the PHE.

In conclusion, we have shown that a simple tight-binding model, which includes the on-site SO coupling, is able to explain the main features of the low temperature AMR in single crystal manganite films, including the dependence of the AMR on the direction of the current to the crystalline axes.

Since the mechanism of transport in manganites is complicated by polaronic effects, extension of the present model to higher temperatures is far from straightforward. Furthermore, comparison with experiments is complicated by the variety of methods of preparation of thin films on different substrates.

We hope that the measurements and calculations presented here will serve as a starting point and promote future research on the fundamental aspects of AMR in manganites.

References

[1] Jin S, Tiefel T H, McCormack M, Fastnacht R A, Ramesh R and Chen L H 1994 *Science* **264** 413
[2] Hwang H Y, Cheong S-W, Ong N P and Batlogg B 1996 *Phys. Rev. Lett.* **77** 2041
[3] Coey J M D, Viret M and von Molnar S 1999 *Adv. Phys.* **48** 167
[4] Dagotto E, Hotta T and Moreo A 2001 *Phys. Rep.* **344** 1
[5] Israel C, Calderón M J and Mathur N D 2007 *Mater. Today* **10** 24
[6] Ziese M and Sena S P 1998 *J. Phys.: Condens. Matter* **10** 2727
[7] Bason Y, Klein L, Yau J-B, Hong X and Ahn C H 2004 *Appl. Phys. Lett.* **84** 2593

[8] Bibes M, Laukhin V, Valencia S, Martínez B, Fontcuberta J, Gorbenko O Yu, Kaul A R and Martínez J L 2005 *J. Phys.: Condens. Matter* **17** 2733

[9] Infante I C, Hrabovský D, Laukhin V, Sánchez F and Fontcuberta J 2006 *J. Appl. Phys.* **99** 08c502

[10] Yau J-B, Hong X, Posadas A, Ahn C H, Gao W, Altman E, Bason Y and Klein L 2007 *J. Appl. Phys.* **102** 103901

[11] Bason Y, Hoffman J, Ahn C H and Klein L 2009 *Phys. Rev. B* **79** 092406

[12] Campbell I A and Fert A 1982 *Ferromagnetic Materials* vol 3 (Amsterdam: North-Holland) chapter 9

[13] Campbell I A, Fert A and Jaoul O 1970 *J. Phys. C: Solid State Phys.* **3** S95

[14] Urushibara A, Moritomo Y, Arima T, Asamitsu A, Kido G and Tokura Y 1995 *Phys. Rev. B* **51** 14103

[15] Rojas Sánchez J C, Granada M, Steren L B, Mazzaro I and Mosca D H 2007 *Appl. Surf. Sci.* **254** 219

[16] Granada M 2007 *PhD Thesis* Universidad Nacional de Cuyo Instituo Balseiro

[17] Fuhr J D, Avignon M and Alascio B 2008 *Phys. Rev. Lett.* **100** 216402

[18] Saitoh T, Bocquet A E, Mizokawa T, Namatame H, Fujimori A, Abbate M, Takeda Y and Takano M 1995 *Phys. Rev. B* **51** 13942

[19] Ziman J M 1962 *Electrons and Phonons* (Oxford: Oxford University Press)